Electronic Supplementary Information for

A Simple and Highly Selective 2,2-diferrocenylpropane-based Multi-channel Ion Pair Receptor for Pb^{2+} and HSO_4^-

Qian Wan[a], Ji-Bin Zhuo[a], Xiao-Xue Wang[a], Cai-Xia Lin[a,*] and Yao-Feng Yuan[a,b,**]

[a] Department of Chemistry, Fuzhou University, Fuzhou 350116, China

[b] State Key Laboratory of Photocatalysis on Energy and Environment, Fuzhou University, Fuzhou 350002, China

*Corresponding author. Tel./Fax: +86-591-22866161; E-mail: LCX395314748@163.com *(C.-X. Lin).*

**Corresponding author. Tel./Fax: +86-591-22866161; E-mail: yaofeng_yuan@fzu.edu.cn *(Y.-F. Yuan).*

Table of Contents

1. Materials and instruments

All of the starting materials were obtained from commercial suppliers and used without further purification. All reactions were performed under the nitrogen atmosphere, the solvents were dried by standard methods and then distilled prior to use. NMR spectra were recorded on a Bruker Avance III 400 NMR apparatus. High-resolution mass spectra (HRMS) were obtained on a Bruker En Apex ultra 7.0 FT-MS spectrometer. Melting points were determined with a 4X microscopic melting point instrument. The UV-visible spectra were measured on a Perkin Elmer lambda 750UV/VIS/NIR spectrometer. Fluorescence spectra were collected on an Edinburgh FL-FS 920 TCSPC. Fluorescence images were obtained on a CEL-M 500 high-pressure mercury lamp. X-ray structural measurements were carried out with a Rigaku RAXISIV CCD diffract meter with a graphite-monochromator Mo-Kα radiation (λ= 0.071073 nm) at 293(2) K. All diffraction data were collected by scanning in a certain mode and refined in Lp factor. Theoretical calculation for the geometrical optimization of receptor **1** and complex **1**·Pb^{2+} was performed at the density functional theory (DFT) level using the B3LYP hybrid functional. The 6-31G and 6-31G(d) basis sets were employed for H and C atoms, aug-cc-pVTZ for N atom and LANL2DZ with effective core potential for Fe and Pb atom, respectively. In addition, the energy of the receptor **1** and complex **1**·Pb^{2+} were -41493.6 eV and -41575.2 eV, respectively. After obtaining the optimized structure, the further time-dependent density functional theory (TD-DFT) calculation was performed to investigate the excited states of receptor **1**. All calculations were performed using the Gaussian 09 package.[1]

Cyclic voltammetry (CV) and Differential pulse voltammetry (DPV) studies were performed by CHI620C electrochemical workstation with a conventional three-electrode configuration, glassy carbon as the working electrode, platinum electrode as counter electrode, and Ag/AgCl (3.0 M KCl) as reference electrode at room temperature (scan rate: 100 mV/ s). The experiments were carried out with a 2×10^{-4} M solution of receptor **1** in CH_3CN containing 0.1 M $(n\text{-}C_4H_9)_4ClO_4$ (TBAP) as supporting electrolyte for cations, $[n\text{-}Bu_4N]PF_6$ ($TBAPF_6$) (c = 0.10 M) for anions.

2. Synthesis details and characteristic data

2.1 The Synthetic routine of **1**

In a 100 mL round bottom flask 2,2-Diferrocenylpropanecarbaldehyde **2** (510 mg, 1.2 mmol) and 2,3-diaminopyridine **3** (200 mg, 1.9 mmol) were dissolved in MeOH (60 mL). Iodine was added into the solution for initiating the reaction. The mixture was stirred at reflux 24 h under nitrogen atomosphere to complete the reaction which was monitored by TLC. The reaction mixture obtained was allowed to cool to room temperature and solvent was evaporated under reduced pressure to give the residue. The residue was redissolved in dichloromethane and washed with saturated NaS_2O_4 until colorless in the aqueous layer. Then the organic layer was washed with saturated NaCl, dried over Na_2SO_4 and concentrated to give the crude product, which was further purified by column chromatography over basic alumina using petroleum ether/ethyl acetate (2:1) mixture as eluent to give receptor **1** as a yellow solid (235mg, Yield = 38.6%). mp: >200 °C. Anal. Found: C, 65.69, H, 5.39, N, 7.88. Calc. for $C_{29}H_{27}Fe_2N_3$ (529.09): C, 65.81; H, 5.14; N, 7.94%. IR (KBr) ν_{max}/cm^{-1}：3096, 2968, 1562, 1404, 1330, 1271, 1032, 818, 777; ^1H NMR δ_H (400 MHz, DMSO-d_6,) 12.98 (1H, s , NH), 8.25 (1H, d, J = 3.8 Hz, Py-H), 7.88 (1H, d, J = 7.2 Hz, Py-H), 7.17 (1H, dd, J = 7.7, 4.8 Hz, Py-H), 5.07-3.94 (m, 17H, Cp-H), 1.55 (s, 6H, Me). ^{13}C NMR δ (101 MHz, DMSO-d_6, Me_4Si) 103.10, 101.37, 73.77, 71.28, 69.10, 68.54, 68.41, 67.52. 66.89, 65.93, 33.04, 30.14. HRMS (ESI): Found: 530.0972, Calc. for $C_{29}H_{27}Fe_2N_3$ $[M+H]^+$: 530.0982.

2.2 Characteristic data

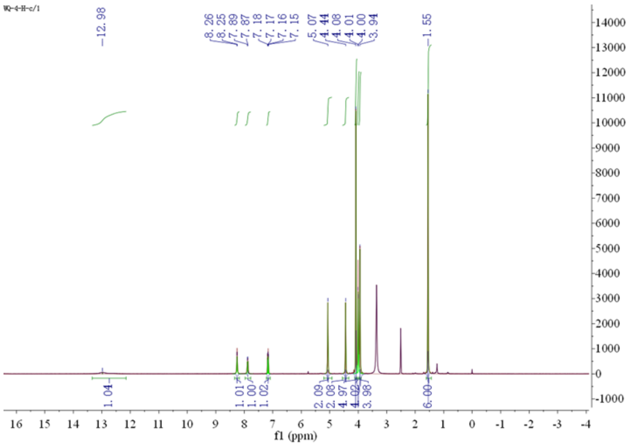

Fig. S1 ^1H NMR spectrum of **1** in DMSO-d_6

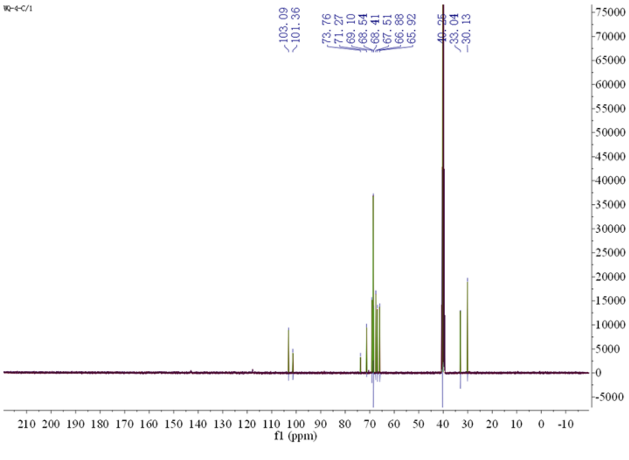

Fig. S2 ^{13}C NMR spectrum of **1** in DMSO-d_6

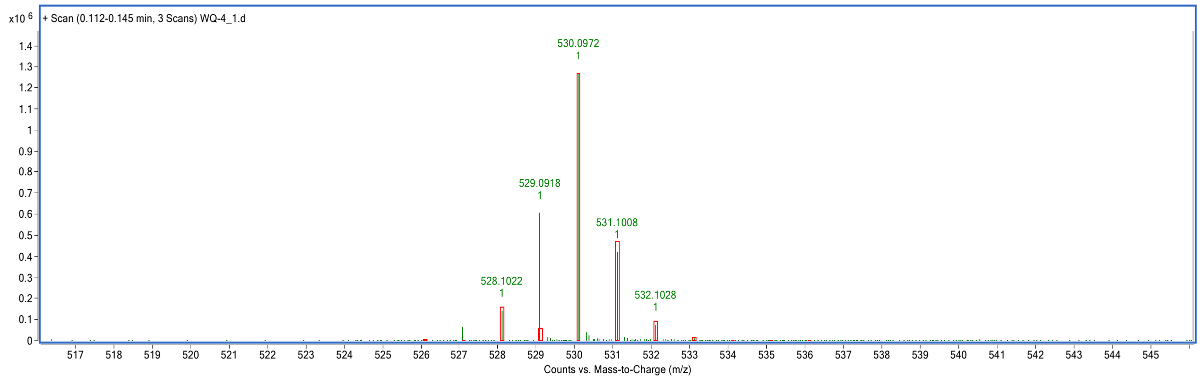

Fig. S3 HRMS spectrum (ESI positive ion) of **1**

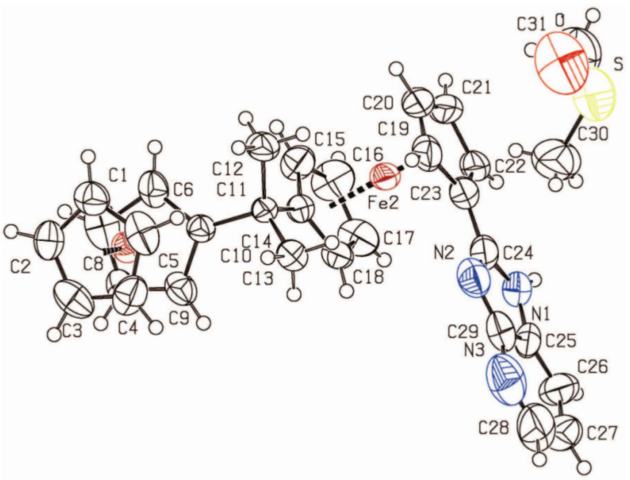

Fig. S4 ORTEP of **1** (thermal ellipsoids were set at 50% probability).

3. Optical Spectroscopy Data

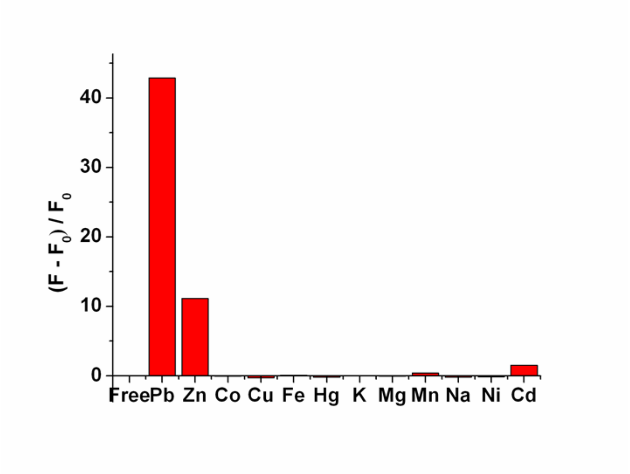

Fig. S5 Fluorescent response of **1** to metal cations, $(F{-}F_0)/F_0$ was calculated according to the emission at 420 nm.

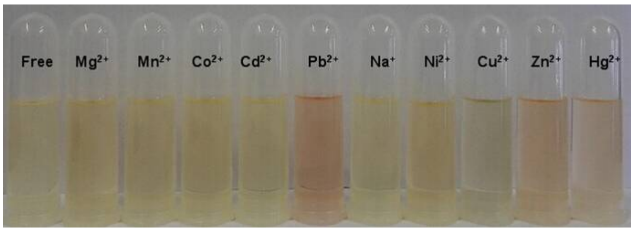

Fig. S6 Visual features observed in CH_3CN solutions of **1** (1 × 10^{-4} M) towards metal cations**.**

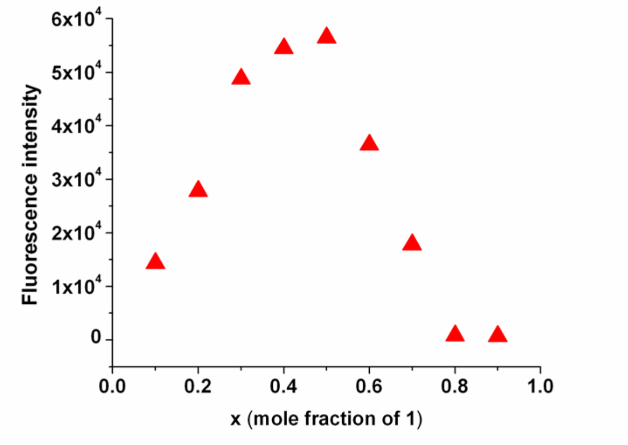

Fig. S7 Job's plots for the binding of **1** with Pb^{2+} using fluorescence method, λ_{ex} = 350 nm and λ_{em} =420 nm.

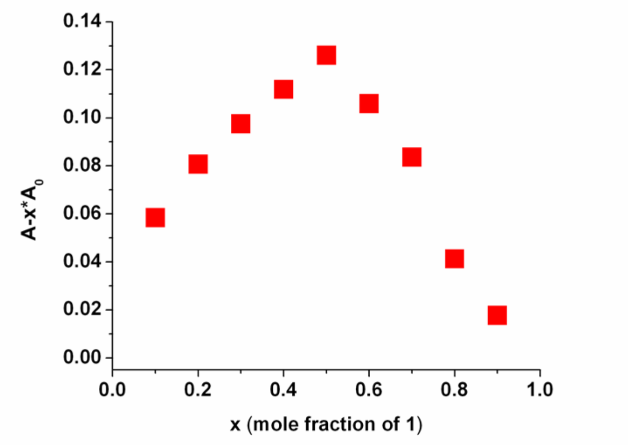

Fig. S8 Job's plots for the binding of **1** with Zn^{2+} using Absorption spectra, absorption at 311 nm.

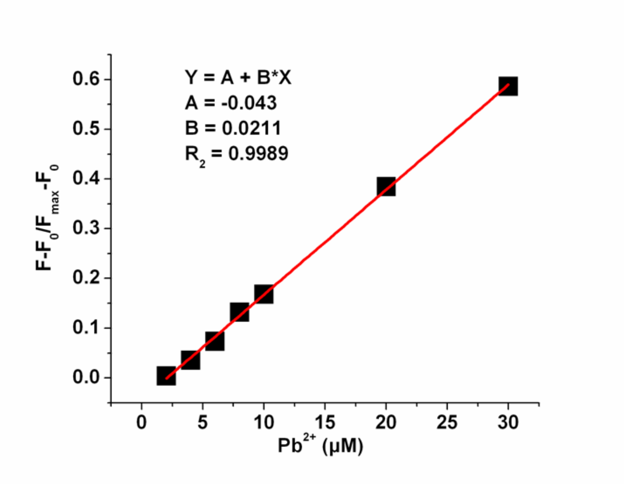

Fig. S9 Determination of association constant of **1** for Pb^{2+} in CH_3CN, $\lambda_{ex} = 350$ nm, $\lambda_{em} =420$ nm.

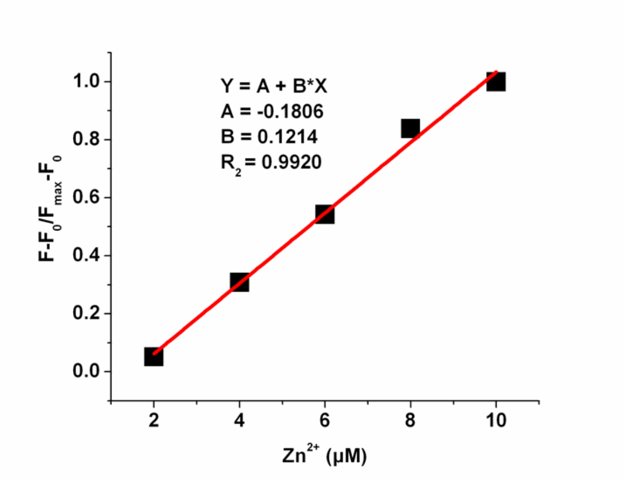

Fig. S10 Determination of association constant of **1** for Zn^{2+} in CH_3CN, $\lambda_{ex} = 350$ nm, $\lambda_{em} =420$ nm, $K_a = 1.21 \times 10^5$ M^{-1}.

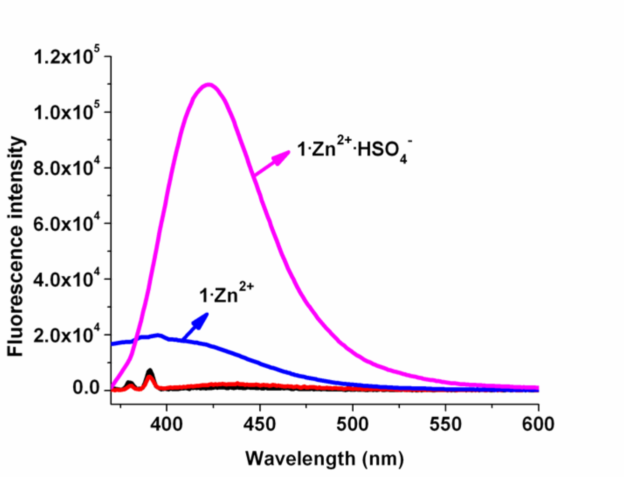

Fig. S11 Fluorescence spectra of **1**, **1**$\cdot HSO_4^-$, **1**$\cdot Zn^{2+}$ and **1**$\cdot Zn^{2+}\cdot HSO_4^-$ (10 μM), excited at 350 nm.

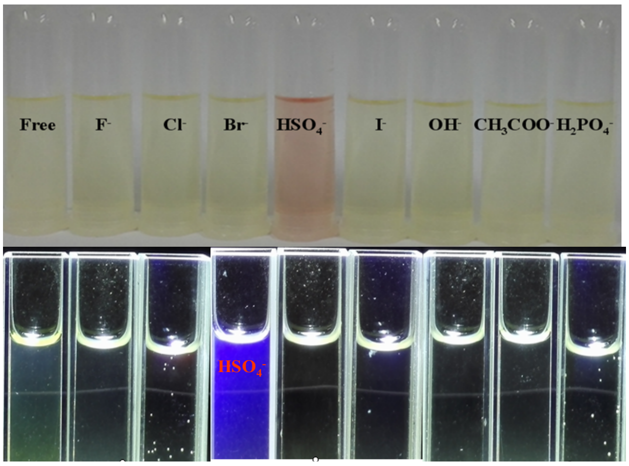

Fig. S12 Color changes of complex **1**·Pb^{2+} (1 × 10^{-4} M) in the presence of 2 equiv. corresponding anions: naked eye (top); under mercury lamp (bottom) in CH$_3$CN.

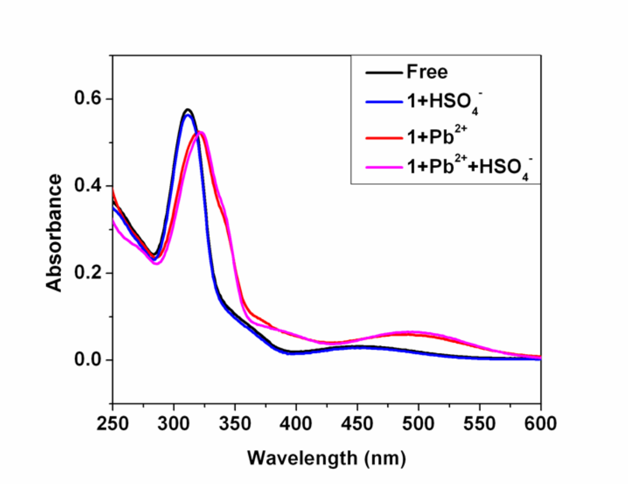

Fig. S13 Changes in the absorption spectra of **1** (2.5 × 10^{-5} M) in CH$_3$CN upon addition of HSO$_4^-$, Pb^{2+}, Pb^{2+} and HSO$_4^-$.

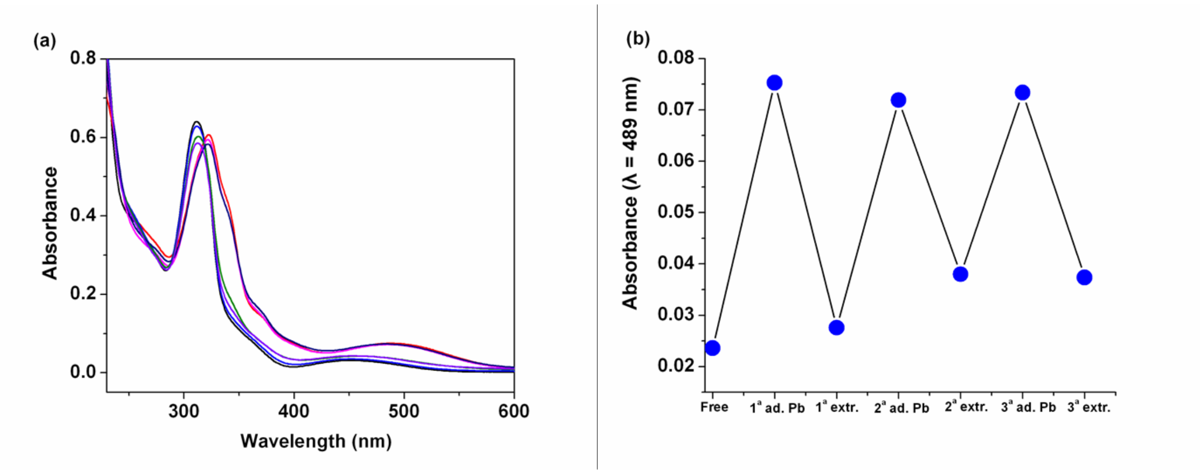

Fig. S14 Stepwise complexation/decomplexation cycles of receptor **1** (2.5 × 10^{-5} M in CH$_3$CN) and Pb^{2+} using [*n*-Bu$_4$N]F as decomplexation agent; carried out by UV/Vis analysis.

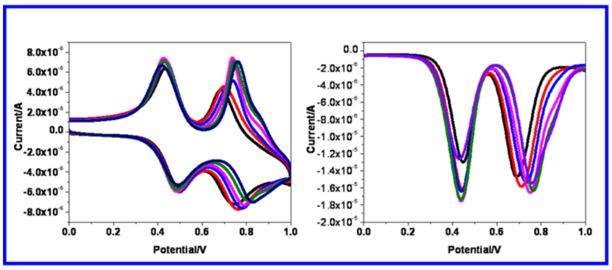

Fig. S15 Evolution of the CV (left) and DPV (right) of **1** (2×10^{-4} M) in CH_2Cl_2 when Zn^{2+} is added: from 0 to 2 equiv.

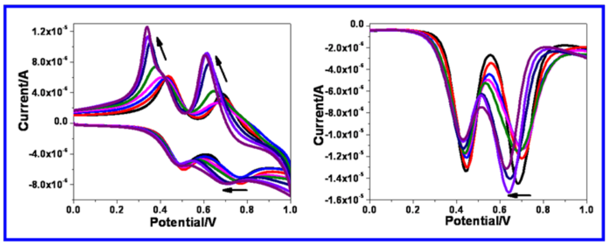

Fig. S16 Evolution of the CV (left) and DPV (right) of **1** (2×10^{-4} M) in CH_2Cl_2 when 8 equiv. HSO_4^- is added.

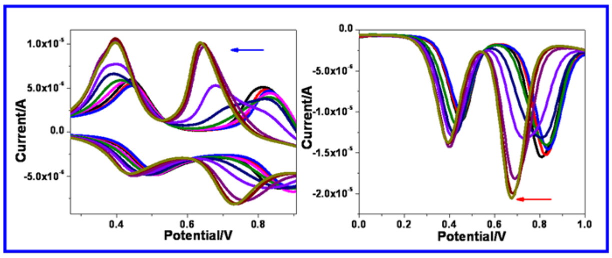

Fig. S17 Evolution of the CV (left) and DPV (right) of **1**·Pb^{2+} in CH_2Cl_2 by gradually addition of HSO_4^- up to 10 equiv.

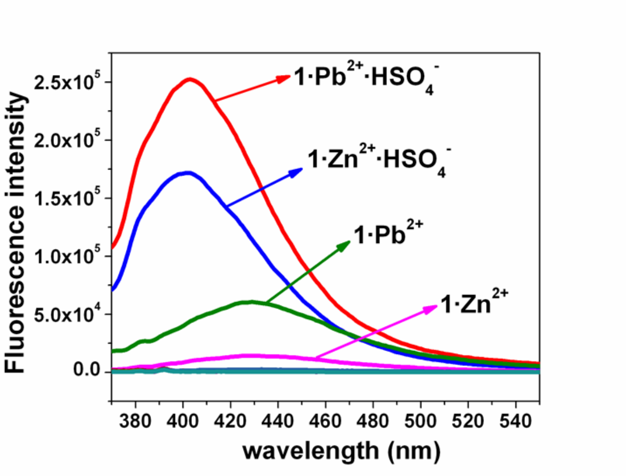

Fig. S18 Fluorescence spectra of **1**, **1**·Pb^{2+} **1**·Pb·HSO_4^-**,** **1**·Zn^{2+} and **1**·Zn^{2+}·HSO_4^- (10 μM) in $CHCl_3$, excited at 350 nm.

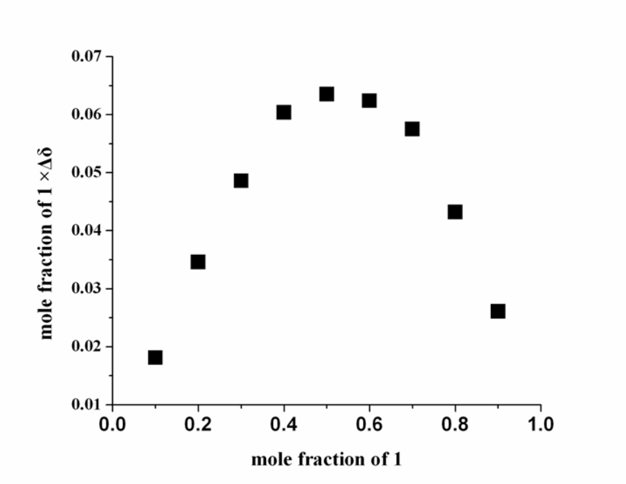

Fig. S19 Job's plots for receptor **1** with HSO_4^- in $CDCl_3$ by monitoring the H2 proton of pyridine ring.

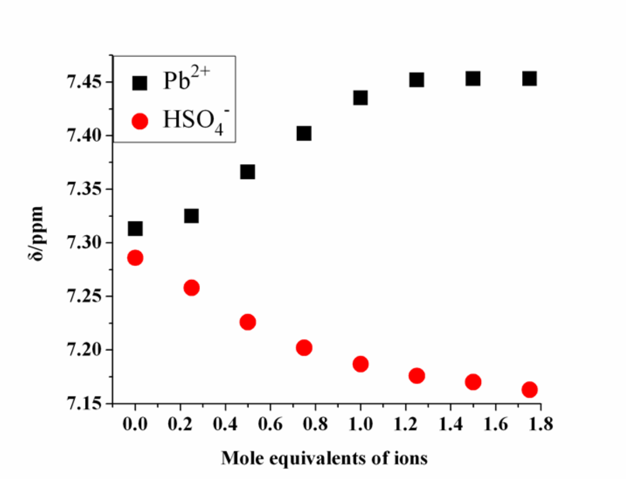

Fig. S20 ^{1}H NMR titration curves of receptor **1** in $CDCl_3$ by monitoring the H2 proton of pyridine ring.

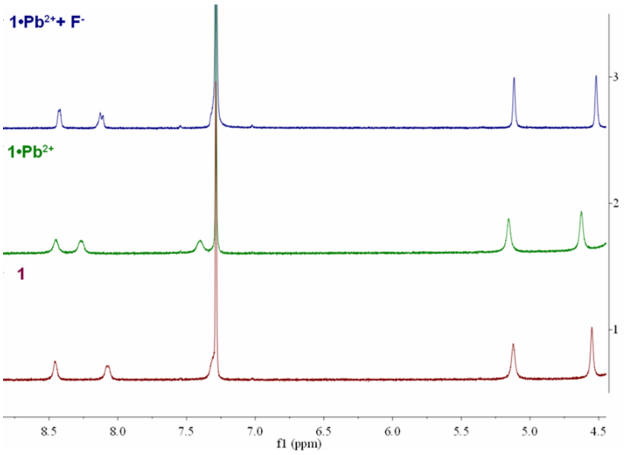

Fig. S21 Complexation/decomplexation process for receptor **1** (6.61 × 10^{-3} M) using [*n*-Bu_4N]F as decomplexation agent, carried out by ^{1}H NMR analysis in $CDCl_3$.

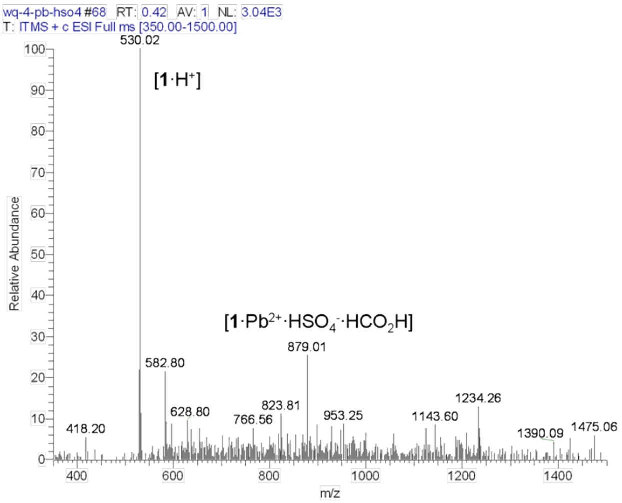

Fig. S22 Mass spectra of receptor **1** upon addition of Pb^{2+} and HSO_4^- in CH_3CN.

Table S1. Selected data of electronic transitions in **1** by TD-DFT calculations using B3LYP/Gen method.

λ[nm/(eV)]	*f*ᵃ	Composition of bands and CIᵇ coefficients
495 (2.50)	0.0037	H-3→L+1, 0.16
488 (2.54)	0.0011	H-2→L+1, 0.14
311 (3.98)	0.1104	H-2→L, 0.21; H-2→L+2, 0.18
288 (4.29)	0.4602	H-4→L, 0.40
286 (4.33)	0.018	H→L+1, 0.40

[a] *f*- oscillator strength; [b] CI- configurational intergration coefficient, H - HOMO, L - LUMO.

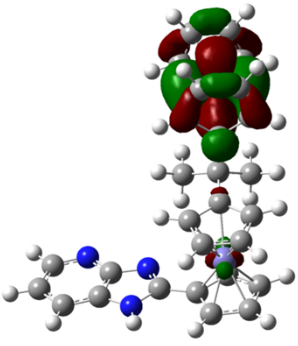
HOMO

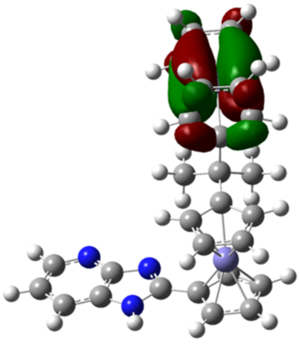
HOMO-1

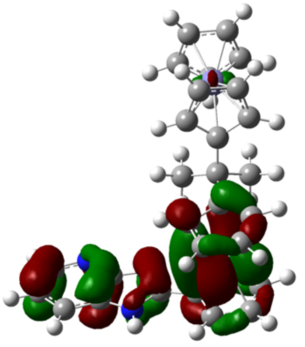
HOMO-2

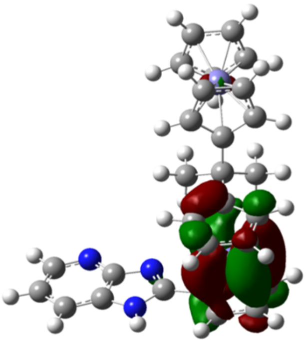
HOMO-3

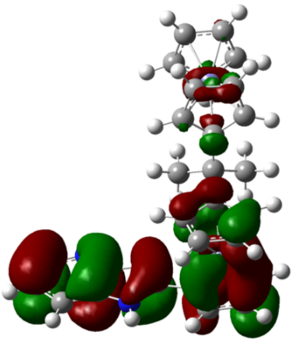
HOMO-4

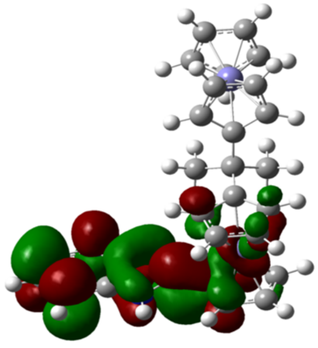
LUMO

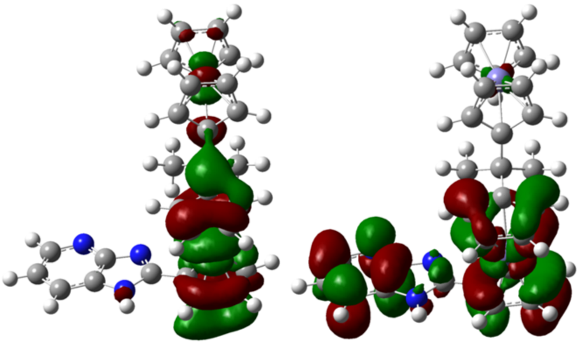

LUMO+1 LUMO+2

Fig. S23 Frontier molecular orbitals of **1** contributing to UV-visible absorption bands.

Table S2. Evolution of ^{1}HNMR data for marked H in the presence of several anions and cations.

	H1 **(Δ δ)**	**H2** **(Δ δ)**	**H3** **(Δ δ)**	**Hα** **(Δ δ)**	**Hβ** **(Δ δ)**
1	8.478	7.310	8.060	5.093	4.553
1·Zn^{2+}	8.515 (+0.037)	7.285 (—0.025)	8.094 (+0.034)	4.722 (—0.371)	4.392 (—0.161)
1·Pb^{2+}	8.359 (—0.119)	7.452 (+0.142)	8.332 (+0.272)	5.269 (+0.176)	4.782 (+0.229)
1·HSO$_4^-$	8.230 (—0.248)	7.181 (—0.129)	8.039 (—0.021)	5.112 (+0.019)	4.413 (—0.140)
1·Pb^{2+}·HSO$_4^-$	8.344 (—0.134)	7.285 (—0.025)	8.344 (+0.284)	5.246 (+0.153)	4.469 (—0.084)

Table S3.Crystallographic data and structure refinement parameters.

Complex	**1**
Empirical formula	$C_{31}H_{33}Fe_2N_3OS$
Formula weight	607.36
Temperature (K)	293(2)
Wavelength (Å)	0.71073
Crystal system	Monoclinic
Space group	*P21/n*
a (Å)	11.1271(7)
b (Å)	19.1069(12)
c (Å)	13.0946(10)
α (°)	90.00
β (°)	94.223(5)
γ (°)	90.00
V (Å^3)	2776.4(3)
Z	4
D_{calc} (g·cm^{-3})	1.453
$F(000)$	1264
Crystal size (mm)	0.50 × 0.40 × 0.20
Index ranges	$-14 \leq h \leq 14$, $-24 \leq k \leq 24$, $-17 \leq l \leq 17$
Reflections collected	21944
Independent reflections	5282 $R_{All} = 0.0429$
Data Completeness	0.987
Refinement method	Full-matrix least-squares on F^2
Final R indices [$I > 2\sigma(I)$]	$R_1 = 0.1268$, $wR_2 = 0.3388$
R indices (all data)	$R_1 = 0.1422$, $wR_2 = 0.3465$
Goodness-of-fit on F^2	2.217

Table S4. Selected bond lengths (Å) and angles (^{o}) for **1.**

bond	**(Å)**	**bond**	**(Å)**
N1—C25	1.363(10)	C10—C11	1.533(8)
N1—C24	1.391(10)	C11—C13	1.535(8)
N2—C24	1.316(11)	C11—C12	1.540(9)
N2—C29	1.346(11)	C11—C14	1.540(9)
N3—C28	1.308(18)	C22—C23	1.433(13)
N3—C29	1.392(15)	C23—C24	1.467(11)
Angles	**(^{o})**	**Angles**	**(^{o})**
C25—N1—C24	104.8(7)	C13—C11—	110.3(5)
C24—N2—C29	105.4(8)	C14—C11—	110.7(5)
C28—N3—C29	118.6(11)	C10—C11—	104.7(5)
C13—C11—	110.2(6)	N2—C24—N1	113.2(8)
C10—C11—	111.4(5)	N2—C24—C23	127.3(8)
C10—C11—	109.5(5)	N1—C24—C23	119.7(8)

References

[S1] M. J. Frisch, G. W. Trucks, H. B. Schlegel, G. E. Scuseria, M. A. Robb, J. R. Cheeseman, G. Scalmani, V. Barone, B. Mennucci, G. A. Petersson, H. Nakatsuji, M. Caricato, X. Li, H. P. Hratchian, A. F. Izmaylow, J. L. Sonnenberg, M. Hada, M. Ehara, K. Toyota, R. Fukuda, J. Hasegawa, M. Ishida, T. Nakajima, Y. Honda, O. Kitao, H. Nakai, T. Vreven, J. A. Montgomery Jr, J. E. Peralta, F. Ogliaro, M. Bearpark, J. J. Heyd, E. Brothers, K. N. Kudin, V. N. Staroverov, R. Kobayashi, J. Normand, K. Raghavachari, A. Rendell, J. C. Burant, S. S. Iyengar, J. Tomasi, M. Cossi, N. Rega, J. M. Millam, M. Klene, J. E. Knox, J. B. Cross, V. Bakken, C. Adamo, J. Jaramillo, R. Gomperts, R. E. Stratmann, O. Yazyev, A. J. Austin, R. Cammi, C. Pomelli, J. W. Ochterski, R. L. Martin, K. Morokuma, V. G. Zakrzewski, G. A. Voth, P. Salvador, J. J. Dannenberg, S. Dannenberg, S. Dapprich, A. D. Daniels, O. Farkas, J. B. Foresman, J. V. Ortiz, J. Cioslowski and D. J. Fox, Gaussian 09, Revision A.1, Gaussian, Inc., Wallingford CT, 2009.